Coulomb drag between a carbon nanotube and monolayer graphene

S. M. Badalyan◉

Center for Graphene Research, Frisco, Texas 75035, USA

A. P. Jauho◉

Center for Nanostructured Graphene, Technical University of Denmark, 2800 Kongens Lyngby, Denmark

We study Coulomb drag in a system consisting of a carbon nanotube and monolayer graphene. Within the Fermi liquid theory, we calculate the drag resistivity and find that the dimensional mismatch of the system components leads to a dependence of the drag rate on the carrier density, temperature, and spacing, which is substantially different from what is known for graphene double layers. Because of the competing effects of forward and backward scattering, we identify features of the drag dependence on the electron density, which allows us to control their relative contribution to the drag resistivity.

I. INTRODUCTION

Coulomb drag in double-well systems has been of considerable theoretical and experimental interest for several decades. The emergence of graphene has significantly expanded the physical regimes in drag experiments [1]. In particular, the insulating barrier between the subsystems can have a thickness down to a few atomic layers, which makes the interaction phenomena more pronounced and gives access to physics [2–6] which is unattainable in semiconductor samples.

Many recent works address Coulomb drag in dimensionally symmetric graphene-based structures: drag between two graphene layers has been studied both experimentally and theoretically [7–15]. Coupled one-dimensional systems have been also considered [16,17]. Clearly, the drag properties depend essentially on the system dimensionality. One may thus expect that a dimensional *mismatch* of the electronic subsystems can significantly affect Coulomb correlations and characteristics of the drag resistance. Until recently, however, drag between dimensionally mismatched subsystems has attracted less attention and has been limited to a few theoretical works on conventional systems [18,19].

The recent experimental realization of graphene-based dimensionally mismatched electronic structures between a carbon nanotube (CNT) and a graphene monolayer [20] acts as an excellent stimulus for further experimental and theoretical work in this interesting direction. The plasmon spectrum in systems of Coulomb coupled graphene nanoribbon and monolayer graphene has been recently calculated [21,22]. It is predicted that due to the strong interlayer Coulomb coupling, these hybrid systems behave effectively as one dimensional (1D) and do not support two dimensional (2D) plasmon modes with a square-root dispersion [21].

In the present paper, we study Coulomb drag in dimensionally mismatched graphene systems, consisting of either a metallic or a semiconducting CNT and monolayer graphene. Adopting the Fermi liquid theory [23], we calculate the dependence of the drag resistivity on the carrier density, temperature, and spacing between the CNT and graphene. We find that the screening effect, taken into account within the random phase approximation (RPA), strongly suppresses the drag rate and qualitatively changes its dependence on the system parameters. The dimensional mismatch leads to a dependence of the drag resistivity on the carrier density, temperature, and spacing, which differs substantially from that known for symmetric 2D-2D or 1D-1D electronic systems. Meanwhile, the temperature and spacing dependence is found to be rather close to the behavior obtained in Ref. [19] for conventional 1D-2D systems. We also show that the transresistivity for systems with a semiconducting CNT exhibits a slight dip or upturn depending, respectively, on the carrier density in a CNT or graphene, at densities corresponding to the matched Fermi wave vectors. This is because the 2D momentum is not conserved in this hybrid system and the backscattering events, which are, in general, possible in semiconducting CNTs, are suppressed due to the presence of graphene. Thus, these distinctive features in the density dependence of the drag resistivity allow us to distinguish and tune the backward and forward scattering contributions to 1D-2D drag.

II. THEORETICAL MODEL

We consider the following geometry (cf. Fig. 1). A carbon nanotube of radius R is separated by a barrier of thickness d from a graphene monolayer. The system has translational
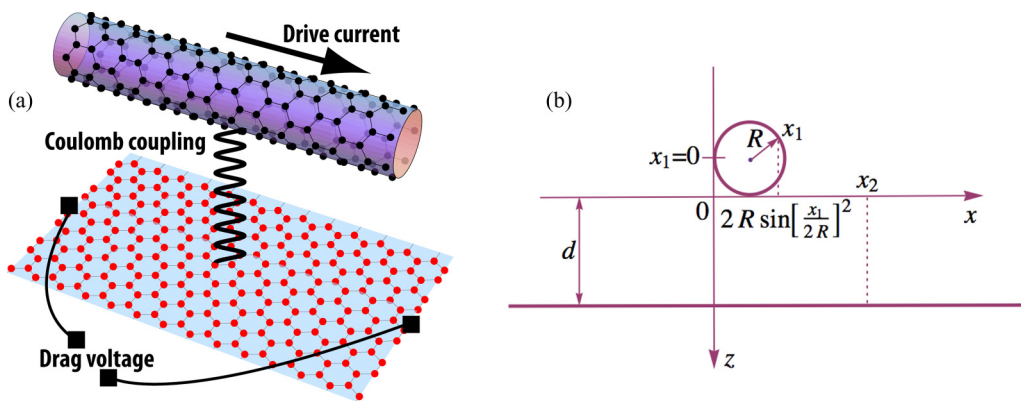
FIG. 1. (a) Schematic view of frictional Coulomb drag in a dimensionally mismatched graphene system. (b) Details of the geometry: the bold lines show the x-z profile of Coulomb coupled carbon nanotube (metallic or semiconducting) of the radius R and monolayer graphene, separated by a barrier with the ϵ_{eff} dielectric constant and of the thickness d along the z direction. The $0 \leqslant x_1 \leqslant 2\pi R$ and $-\infty < x_2 < +\infty$ coordinates correspond, respectively, to the electron positions on the cylindrical surface of CNT and on the plane of graphene.

invariance only along the y direction. The electronic states in the CNT are described by the quantum numbers n, ν, s, k, where the transverse quantization subband index is an integer, $n = 0, \pm 1, \ldots$; ν refers to the type of CNT ($\nu = 0$ refers to metallic nanotubes, both armchair and zigzag, while $\nu = \pm 1$ correspond to semiconducting zigzag nanotubes). The chirality index s describes the conduction ($s = +1$) and valence ($s = -1$) bands, and k is the conserved wave vector along the y direction. The single-particle energy spectrum in CNT $\varepsilon_{1D}^{n,\nu}(s, k) = s\hbar v_{\text{gr}}\sqrt{k_{n,\nu}^2 + k^2}$, where $k_{n,\nu} = (n - \frac{\nu}{3})/R$ and v_{gr} is the electron velocity in graphene [28]. In monolayer graphene, the quantum numbers $(s, \vec{p})$ describe the 2D electron spinor states in the (x, y) plane with the in-plane momentum $\vec{p}$ and the single-particle Dirac spectrum $\varepsilon_{2D}(s, |\vec{p}|) = s v_{\text{gr}} p$. In the present work, we assume spin and valley degeneracy with the degeneracy factors $g_s = 2$ and $g_v = 2$ (interlayer Coulomb interaction is small for intervalley electronic transitions because of the large values of the transferred momentum) and restrict ourselves to the consideration of low temperatures and low levels of doping.

In a metallic (semiconducting) CNT with a 1D carrier density $n_{1D} \equiv \frac{N}{L} = 2\pi R n_{2D} \approx 1.9 \times 10^6$ cm^{-1}, corresponding to the areal density $n_{2D} \equiv \frac{N}{L^2} = 3 \times 10^{12}$ cm^{-2} in graphene and to the tube radius $R = 1$ nm, we find the 1D Fermi energy $\varepsilon_F^{1D} \approx 1128.8$ K (250.7 K). Here N is the number of carriers in CNT or graphene. Instead, for $n_{2D} = 3 \times 10^{11}$ cm^{-2} taking the Fermi energies in metallic (semiconducting) CNT and graphene equal, $\varepsilon_F^{1D} = \varepsilon_F^{2D} = 740.2$ K, we have $n_{1D} \approx 1.24 \times 10^6$ cm^{-1} (3.24×10^6 cm^{-1}). Note that $\varepsilon_F^{1D} \propto n_{1D}$ or n_{1D}^2 and $\varepsilon_F^{2D} \propto \sqrt{n_{2D}}$, respectively, in a metallic or semiconducting CNT and in monolayer graphene. On the other hand, the lowest intersubband gap between the $n = +1$ and $n = 0$ energy levels is $\Delta\varepsilon_{1D}^0 = \hbar v_{\text{gr}}/R \approx 7624.5$ K in metallic CNT while $\Delta\varepsilon_{1D}^1 = \hbar v_{\text{gr}}/3R \approx 2541.5$ K in semiconducting CNT. Thus, with these values the Fermi energies and temperatures are smaller than the transverse quantization energy, $\varepsilon_F^{1D}, T \ll \Delta\varepsilon_{1D}^\nu$, so that electronic transitions to the higher energy subbands do not make a significant contribution to drag. We adopt this lowest subband approximation in CNT and thus omit the subband index n.

III. DRAG RESISTANCE

The drag resistance R_D in the CNT-graphene systems can be measured in two different configurations. In the first one, a current I_G flowing through the graphene monolayer induces a voltage V_{CNT} along the nanotube. Then, assuming that the normalization length, L, is the same along the wire and in both x and y directions in graphene, the drag resistance $R_D^{2D-1D} = V_{\text{CNT}}/I_G = \rho_{2D-1D}$ is given just by the transresistivity ρ_{2D-1D}. In the second configuration, the roles of CNT and graphene are switched, and the transresistance is determined as $R_D^{1D-2D} = V_G/I_{\text{CNT}} = \rho_{1D-2D}L/2\pi R$. Thus, because of the asymmetry of the CNT-graphene system the drag *resistivity* is different in the two configurations; however, the drag *resistance* measured along the wire or across graphene obeys the Onsager reciprocal relation and is independent of the choice of the configuration: $R_D \equiv R_D^{1D-2D} = R_D^{2D-1D}$.

We shall assume that the electronic system can be described as a Fermi liquid both in graphene and in the CNT. The electrical current in the system is restricted by impurity scattering and we adopt the Boltzmann equation approach [29], treating interlayer interaction perturbatively. From the balance of the carrier distribution due to the external electric field and scattering events, we find the drag resistivity as

$$\rho_{2D-1D}^\nu = \frac{h}{e^2} \frac{1}{n_{1D}n_{2D}T} \frac{1}{L^2} \sum_{\vec{q}} \int d\hbar\omega \frac{v_{12}(q)^2|I(q_x)|^2}{|\epsilon_{1D-2D}(\vec{q}, \omega)|^2}$$
$$\times \frac{\Gamma_{1D}^\nu(q_y, \omega)\Gamma_{2D}(\vec{q}, \omega)}{\sinh(\hbar\omega/2T)^2}. \tag{1}$$

Here $v_{12}(q) = 2\pi e^2 e^{-qd}/q\epsilon_{\text{eff}}$ is the 2D Fourier transform of the bare interlayer Coulomb interaction with $q = \sqrt{q_x^2 + q_y^2}$ and ϵ_{eff} is the effective low-frequency dielectric function of the insulating barrier. The form factor $I(q_x) = e^{iq_x R}J_0(q_x R)$ with $J_0(x)$ the Bessel function of the first kind. We assume that $d \gg R$.

The dynamical screening function of the hybrid 1D-2D electronic system within the random phase approximation is given [19,21] by $\epsilon_{1D-2D}(\vec{q}, \omega) = \epsilon_{1D}^{\text{eff}}(q_y, \omega)\epsilon_{2D}(q, \omega)$, where

$$\epsilon_{1D}^{\text{eff}}(q_y, \omega) = \epsilon_{1D}(q_y, \omega) - Q_{1D-2D}(q_y, \omega)\Pi_{1D}(q_y, \omega) \tag{2}$$

with

$$\mathcal{Q}_{\text{1D-2D}}(q_y, \omega) = \frac{1}{L} \sum_{q_x} \frac{|I(q_x)|^2 v_{12}(q)^2 \Pi_{2D}(q, \omega)}{\epsilon_{2D}(q, \omega)}. \quad (3)$$

The intralayer dynamical screening functions (the Lindhard polarization functions) in 1D [16,17,30,31] and 2D [32–34] electronic systems are, respectively, denoted by $\varepsilon_{1D}(q_y, \omega)$ [$\Pi_{1D}(q_y, \omega)$] and $\varepsilon_{2D}(q, \omega)$ [$\Pi_{2D}(q, \omega)$].

The nonlinear response function in the CNT [16] is

$$\Gamma_{1D}^{\nu}(q_y, \omega)$$

$$= \frac{e}{\pi \hbar \mu_{1D}} \frac{1}{L} \sum_{s,s';k,k'} \delta_{k',k+q_y} F_{1D}^{\nu}(s, k; s', k')$$

$$\times \text{Im} \frac{h_{1D}^{\nu}(s, k; s', k')[f(\varepsilon_{1D}^{\nu}(s', k')) - f(\varepsilon_{1D}^{\nu}(s, k))]}{\varepsilon_{1D}^{\nu}(s, k) - \varepsilon_{1D}^{\nu}(s', k') + \hbar\omega + i0^+}, \quad (4)$$

while for graphene [13,14] it is given by

$$\Gamma_{2D}^{y}(\vec{q}, \omega)$$

$$= \frac{e}{\pi \hbar \mu_{2D}} \frac{1}{L^2} \sum_{s,s';\vec{p},\vec{p}'} \delta_{\vec{p}',\vec{p}+\vec{q}} F_{2D}(s, \vec{p}; s', \vec{p}')$$

$$\times \text{Im} \frac{h_{2D}^{y}(s, p; s', p')[f(\varepsilon_{2D}(s', p')) - f(\varepsilon_{2D}(s, p))]}{\varepsilon_{2D}(s, p) - \varepsilon_{2D}(s', p') + \hbar\omega + i0^+}. \quad (5)$$

Here the spinor overlap factors, stemming from the Coulomb matrix elements, are given in CNT (graphene) by $F_{1D}^{\nu}(s, k; s', k') = (1 + ss' \cos\theta_{kk'}^{\nu})/2$ [$F_{2D}(s, \vec{p}; s', \vec{p}') = (1 + ss' \cos\theta_{\vec{p}\vec{p}'})/2$] with $\theta_{kk'}^{\nu}$ ($\theta_{\vec{p}\vec{p}'}$) the angle between the vectors (k_ν, k) and (k_ν, k') ($\vec{p}$ and $\vec{p}'$). The Fermi functions are given by $f(\varepsilon)$. We introduce also the functions $h_{1D}^{\nu}(s, k; s', k') = \tau_{1D}^{\nu}(k') v_{1D}^{\nu}(s', k') - \tau_{1D}^{\nu}(k) v_{1D}^{\nu}(s, k)$ and $h_{2D}^{y}(s, p; s', p') = \tau_{2D}(p') v_{2D}^{y}(s', p') - \tau_{2D}(p) v_{2D}^{y}(s, p)$ for CNT and graphene. Respectively, the carrier mobilities and velocities are μ_{1D}, $v_{1D}^{\nu}(s, k) = \partial_k \varepsilon_{1D}^{\nu}(s, k)$ and μ_{2D}, $v_{2D}^{y}(s, p) = \partial_{p_y} \varepsilon_{2D}(s, p)$. In contrast to the mobility (a quantity averaged over the carrier energy), the momentum relaxation transport time $\tau(k)$ is a momentum-dependent

quantity, which is linear in the energy for the dominant type of disorder scattering of Dirac electrons in graphene [35]. It has been shown, however, that the energy dependence does not affect calculations of the nonlinear susceptibility in graphene [13,14] and semiconducting CNT [17]; therefore, we evaluate $\tau_{1D}^{\pm 1}(k) = \tau_{1D}^1$ and $\tau_{2D}(p) = \tau_{2D}$ at the Fermi level and view them as constants. However, this approximation is not justified for a metallic CNT where the function $h_{1D}^0(s, k; s', k')$ with the constant relaxation time vanishes for forward scattering events. Therefore, in this case we include the energy dependence of the momentum relaxation time, and assuming the relaxation time is linear in the energy [12], $\tau_{1D}^0(k) = \tilde{\tau}_{1D}^0|k|$, we find $h_{1D}^0(s, k; s', k') = \tilde{\tau}_{1D}^0 v_{gr}(s'k' - sk)$ for a metallic CNT.

IV. LOW-TEMPERATURE REGIME

From here on, we restrict our discussion to the low-temperature regime, $T \ll \varepsilon_F^{1D}, \varepsilon_F^{2D}$. In this case [36], only electronic transitions within the $s = s' = 1$ band contribute to the nonlinear response functions and they can be calculated analytically. In particular, for a metallic CNT [37], we find

$$\Gamma_{1D}^0(q_y, \omega) = \frac{e \tilde{\tau}_{1D}^0}{\hbar \mu_{1D}} \frac{\omega^2}{2\pi \hbar v_{gr}} [\delta(\omega + v_{gr} q_y) - \delta(\omega - v_{gr} q_y)]. \quad (6)$$

The screening function in Eqs. (1)–(3) can be approximated in the static limit, $\epsilon_{\text{1D-2D}}(\vec{q}, 0)$. In graphene, we use the static polarizability $\Pi_{2D}(q, 0) = -2k_F^{2D}/\pi \hbar v_F$ for $q < 2k_F^{2D}$ [32] and we have $\epsilon_{2D}(q, 0) = 1 + 4\alpha_{gr} k_F^{2D}/q$ with $\alpha_{gr} = e^2/\hbar v_F \epsilon_{\text{eff}}$. In numerical calculations, we take $\epsilon_{\text{eff}} = 4$ mimicking a hexagonal-BN barrier. In a metallic CNT, the static polarizability is approximated as $\Pi_{1D}(q_y, 0) = -1/\pi^2 \hbar v_F$ [16,30] while the bare interaction in $\epsilon_{1D}(q, 0)$ is $v_{1D}(q) = 2\hbar v_F \alpha_{gr} I_0(|q_y|R) K_0(|q_y|R)$ [28], and we find $\epsilon_{1D}^{\text{eff}}(q_y, 0)$ as a one-dimensional integral and calculate it numerically. Here $I_0(y)$ and $K_0(y)$ are the modified Bessel functions of the first and second kinds. In a semiconducting CNT, the static polarizability $\Pi_{1D}(q_y, 0)$, according to its definition, is represented as an additional one-dimensional integral in $\epsilon_{1D}^{\text{eff}}(q_y, 0)$.
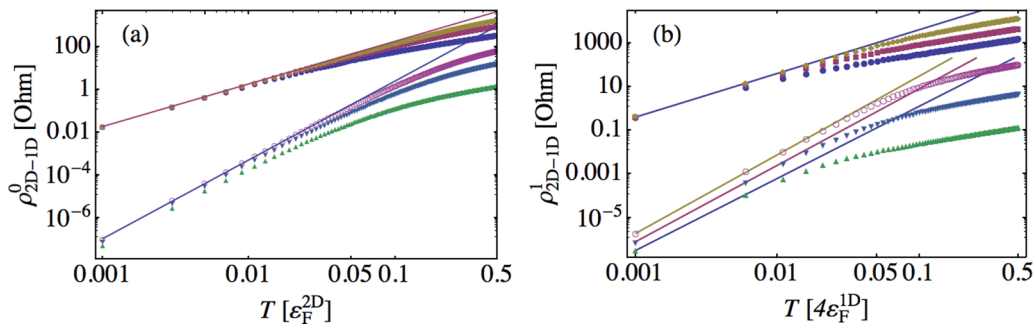
FIG. 2. The temperature dependence of the drag resistivity between (a) a metallic or (b) semiconducting CNT and graphene. Symbols show the transresistivity in the log-log scale with (the lower set) and without (the upper set), including the screening effect for spacing $d = 30$, 10, and 3 nm (down-up). The radius of CNT $R = 1$ nm and the carrier densities $n_{2D} = 3 \times 10^{11}$ cm^{-2} and $n_{1D} = 1.24 \times 10^6$ cm^{-1} ($n_{2D} = 2.7 \times 10^{12}$ cm^{-2} and $n_{1D} = 3.71 \times 10^6$ cm^{-1}) in a metallic (semiconducting) CNT-graphene hybrid system. The solid thin lines represents the T^β power law behavior as a guide to the eye with $\beta = 2$ (the upper set) and $\beta = 3.7$ (the lower set) on the left panel and with $\beta = 2$ (the upper set) and $\beta = 3.3, 3.5$, and 3.6 (the lower set, down-up) on the right panel.
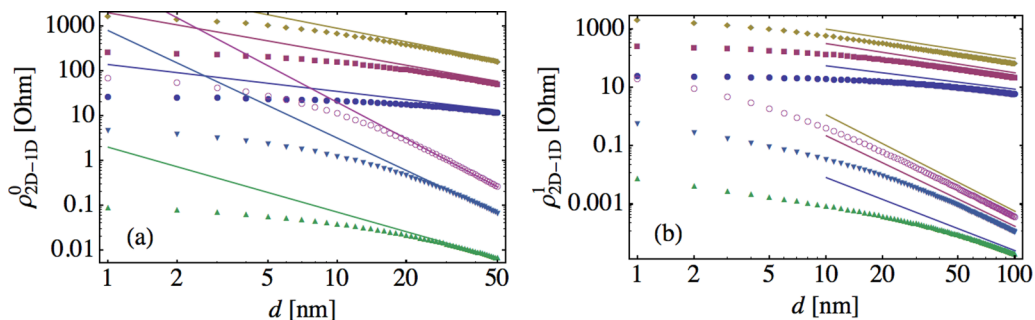
FIG. 3. The drag resistivity between (a) a metallic or (b) semiconducting CNT and graphene as a function of spacing d. Symbols show the transresistivity in the log-log scale with (the lower set) and without (the upper set) including the screening effect at different temperatures $T = 30$, 100, and 300 K (down-up). The other parameters are the same as in Fig. 2. The solid thin lines represent the $d^{-\beta}$ behavior as a guide to the eye with $\beta = 2, 2.7, 3; 0.8, 0.9, 1$ and $\beta = 2.5, 3.1, 3.3; 0.8, 1, 1$ (down-up), respectively, on the left and right panels.

V. NUMERICAL RESULTS AND DISCUSSION

We first discuss the temperature dependence of the drag resistivity between a CNT and graphene. As seen in Fig. 2, the transresistivity without screening shows approximately the familiar T^2 dependence, which originates from the interplay between the 1D-2D phase space behavior in drag scattering events at low T and the long wavelength singularity of the unscreened interaction. In contrast to drag in conventional 2D systems [29], here the integrations over q_x, q_y, and ω are not decoupled into products of one-dimensional integrals. Therefore, the static screening effect, along with the strong suppression of the absolute drag resistivity, changes qualitatively the drag behavior as a function of T and substantially enhances this dependence (cf. Fig. 2). We observe a similar effect also for the interlayer spacing dependence of drag. In the absence of screening, the overall weak dependence on d (cf. Fig. 3) is due to the long wavelength singularity of the unscreened interaction, which is much stronger in this hybrid 1D-2D system than in 1D-1D electronic systems. Even after screening is turned on, the drag resistivity remains a weakly decreasing function with d for small values of $d \lesssim 10$ nm. For relatively large values of $d \gtrsim 50$ nm, the decrease of the drag resistivity becomes rather strong and can be fitted by a power law function $d^{-\beta}$ with $\beta \sim 3$ at $T \gtrsim 300$. The index β decreases with a decrease of T.

Note that the drag resistivity as function of T and d shows a qualitatively similar behavior for metallic and semiconducting CNTs. As seen, however, in Figs. 4 and 5, this is not the case for the drag resistivity as a function of the carrier density. In Fig. 4, we show the drag between a metallic CNT and graphene as a function of the carrier density in graphene. These plots show that the drag resistivity is approximately inversely proportional to $n_{2D}^{1.5}$ and $n_{2D}^{0.5}$, respectively, with and without including the screening effect. We find also that in this low-T regime $\rho_{2D-1D}^1 \propto 1/n_{1D}$. This rather stable density behavior of the transresistivity in a wide range of density variations both in a metallic CNT and graphene is stipulated by the forward scattering events of Dirac electrons.

In the case of a semiconducting CNT and graphene, both forward and backward scattering processes mediate drag and their relative contribution to drag can be controlled by varying the ratio of the carrier densities. In Fig. 5, the vertical thin lines indicate the carrier densities $n_{2D}^* = 2.7 \times 10^{12}$ cm^{-2} (left panel) and $n_{1D}^* = 3.71 \times 10^6$ cm^{-1} (right panel) for matched Fermi wave vectors in graphene and CNT, $k_F^{1D} = k_F^{2D}$. These lines separate different drag scattering regimes. At low densities in graphene, backscattering is suppressed by the presence of a graphene monolayer. Mediated by small-angle scattering events, the drag resistivity decreases with an increase of n_{2D}. We observe, however, that against this overall
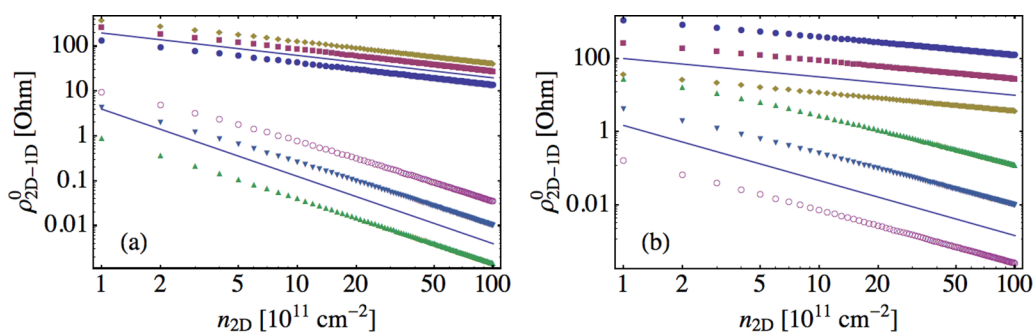
FIG. 4. The dependence of the drag resistivity between a metallic CNT and graphene on the carrier density in graphene (a) for $d = 30$, 10, and 3 nm (down-up) at $T = 100$ K and (b) at $T = 30$, 100, and 300 K (down-up) for $d = 10$ nm. In each panel, the lower (upper) set of symbols show log-log plots of the transresistivity with (without) including the screening effect. The radius of CNT is $R = 1$ nm and the carrier density $n_{1D} = 1.24 \times 10^6$ cm^{-1}. The solid thin lines represent the $n_{2D}^{-0.5}$ (the upper line) and $n_{2D}^{-1.5}$ (the lower line) behaviors as a guide to the eye.
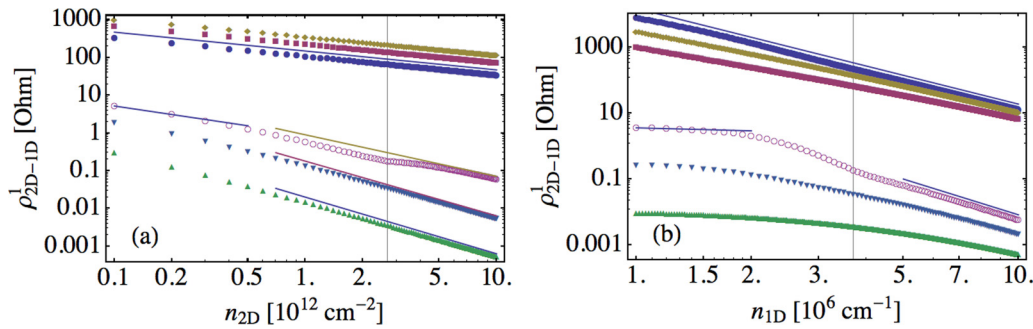
FIG. 5. The dependence of the drag resistivity between a semiconducting CNT and graphene on the carrier density in graphene (a) for a fixed density $n_{1D}^* = 3.71 \times 10^6$ cm^{-1} in the CNT and (b) on the density in the CNT for a fixed density $n_{2D}^* = 2.7 \times 10^{12}$ cm^{-2} in graphene. The symbols are the log-log plots of the transresistivity calculated with (the lower set) and without (the upper set) including the screening effect for $d = 30$, 10, and 3 nm (down-up) at $T = 100$ K. The radius of CNT is $R = 1$ nm. The solid thin lines represent the $n_{2D}^{-\beta_2}$ and $n_{1D}^{-\beta_1}$ behaviors as a guide to the eye, respectively, on the left panel with $\beta_2 = 0.5$ (the upper line) and $\beta_2 = 1.5$, 1.45, 0.9, and 0.75 (the lower lines, down-up) and on the right panel with $\beta_1 = 2.9$ (the upper line) and $\beta_1 = 0.3$ and 3.6 (the lower lines, down-up).

monotonic background, the transresistivity shows a slight dip at the matching density $n_{2D} = n_{2D}^*$ (cf. the left panel in Fig. 5). This feature is due to the backward scattering channel, which opens for $n_{2D} > n_{2D}^*$.

On the right panel in Fig. 5, it is seen that the drag resistivity shows an upward trend as a function of n_{1D}. In this case, backward scattering events become open for densities in CNT smaller than $n_{1D} < n_{1D}^*$, and result in a strengthened enhancement of the drag resistivity with a decrease of n_{1D}. With a further decrease of n_{1D}, the scattering phase space decreases and the dependence of the transresistivity on n_{1D} becomes rather weak. Note that the manifestation of a sequence of different scattering regimes with variation of the carrier densities is more pronounced in samples with small values of the spacing d where backscattering is significant and leads to the interplay of the small and large-angle scattering contributions to the drag resistivity.

VI. CONCLUSIONS

We have worked out the Fermi liquid predictions for a system consisting of a CNT and monolayer graphene. The overall physics is dominated by the dimensionality mismatch.

This leads to a qualitatively novel picture of drag than that of dimensionally symmetric graphene structures. Metallic and semiconducting CNTs show qualitatively different behavior. In particular, in structures consisting of semiconducting CNTs, the drag resistivity exhibits new features due to the competing effects of forward and backward scattering and by adjusting the charge densities one can tune the accessible scattering processes contributing to the drag resistivity. This study paves the way for further exploration of new phenomena induced by the interplay of the fundamental properties of systems, the dimensionality, and interaction, under various physical circumstances. In particular, we briefly mention a few interesting issues as an extension of our results: Coulomb drag at high temperatures; drag between a Luttinger liquid in a CNT and a Fermi liquid in graphene; and the effect of quantizing magnetic fields on drag in hybrid systems.

[1] B. N. Narozhny and A. Levchenko, Rev. Mod. Phys. **88**, 025003 (2016).

[2] J. I. A. Li, T. Taniguchi, K. Watanabe, J. Hone, A. Levchenko, and C. R. Dean, Phys. Rev. Lett. **117**, 046802 (2016).

[3] K. Lee, J. Xue, D. C. Dillen, K. Watanabe, T. Taniguchi, and E. Tutuc, Phys. Rev. Lett. **117**, 046803 (2016).

[4] X. Liu, K. Watanabe, T. Taniguchi, B. I. Halperin, and P. Kim, Nat. Phys. **13**, 746 (2017).

[5] J. I. A. Li, T. Taniguchi, K. Watanabe, J. Hone, and C. R. Dean, Nat. Phys. **13**, 751 (2017).

[6] X. Liu, L. Wang, K. C. Fong, Y. Gao, P. Maher, K. Watanabe, T. Taniguchi, J. Hone, C. Dean, and P. Kim, Phys. Rev. Lett. **119**, 056802 (2017).

[7] S. Kim, I. Jo, J. Nah, Z. Yao, S. K. Banerjee, and E. Tutuc, Phys. Rev. B **83**, 161401(R) (2011).

[8] R. V. Gorbachev, A. K. Geim, M. I. Katsnelson, K. S. Novoselov, T. Tudorovskiy, I. V. Grigorieva, A. H. MacDonald, S. V. Morozov, K. Watanabe, T. Taniguchi, and L. A. Ponomarenko, Nat. Phys. **8**, 896 (2012).

[9] M. Titov, R. V. Gorbachev, B. N. Narozhny, T. Tudorovskiy, M. Schutt, P. M. Ostrovsky, I. V. Gornyi, A. D. Mirlin, M. I. Katsnelson, K. S. Novoselov, A. K. Geim, and L. A. Ponomarenko, Phys. Rev. Lett. **111**, 166601 (2013).

[10] W.-K. Tse, B. Y.-K. Hu, and S. Das Sarma, Phys. Rev. B **76**, 081401(R) (2007).

[11] M. I. Katsnelson, Phys. Rev. B **84**, 041407(R) (2011).

[12] E. H. Hwang, R. Sensarma, and S. Das Sarma, Phys. Rev. B **84**, 245441 (2011).

[13] B. N. Narozhny, M. Titov, I. V. Gornyi, and P. M. Ostrovsky, Phys. Rev. B **85**, 195421 (2012).

[14] M. Carrega, T. Tudorovskiy, A. Principi, M. I. Katsnelson, and M. Polini, New J. Phys. **14**, 063033 (2012).

[15] S. M. Badalyan and F. M. Peeters, Phys. Rev. B **86**, 121405(R) (2012).

[16] A. M. Lunde, K. Flensberg, and A.-P. Jauho, Phys. Rev. B **71**, 125408 (2005).

[17] A. A. Shylau and A.-P. Jauho, Phys. Rev. B **89**, 165421 (2014)

[18] Y. M. Sirenko and P. Vasilopoulos, Phys. Rev. B **46**, 1611 (1992).

[19] S. K. Lyo, Phys. Rev. B **68**, 045310 (2003).

[20] A. Cheng, T. Taniguchi, K. Watanabe, P. Kim, and J.-D. Pillet, Phys. Rev. Lett. **123**, 216804 (2019).

[21] S. M. Badalyan, A. A. Shylau, and A. P. Jauho, Phys. Rev. Lett. **119**, 126801 (2017).

[22] E. H. Hwang, B. Y.-K. Hu, and S. Das Sarma, Phys. Rev. B **98**, 161304(R) (2018).

[23] Currently, to the best of our knowledge, there is no established clear-cut experimental evidence that the drag in quasi-1D systems is determined by a non-Fermi liquid behavior. The presence of many theoretical predictions for Luttinger liquid based drag in double CNTs [24–27] underscores the importance to firmly establish the Fermi liquid picture of the behavior of hybrid graphene systems with quasi-1D CNTs: The hybrid systems are technologically feasible, and experiments are becoming available.

[24] K. Flensberg, Phys. Rev. Lett. **81**, 184 (1998).

[25] V. V. Ponomarenko and D. V. Averin, Phys. Rev. Lett. **85**, 4928 (2000).

[26] A. Komnik and R. Egger, Eur. Phys. J. B **19**, 271 (2001)

[27] M. Pustilnik, E. G. Mishchenko, L. I. Glazman, and A. V. Andreev, Phys. Rev. Lett. **91**, 126805 (2003).

[28] T. Ando, J. Phys. Soc. Jpn. **74**, 777 (2005).

[29] A. P. Jauho and H. Smith, Phys. Rev. B **47**, 4420 (1993).

[30] W. Que, Phys. Rev. B **66**, 193405 (2002).

[31] A. A. Shylau, S. M. Badalyan, F. M. Peeters, and A. P. Jauho, Phys. Rev. B **91**, 205444 (2015).

[32] B. Wunsch, T. Stauber, F. Sols, and F. Guinea, New J. Phys. **8**, 318 (2006).

[33] E. H. Hwang and S. Das Sarma, Phys. Rev. B **75**, 205418 (2007).

[34] V. N. Kotov, B. Uchoa, V. M. Pereira, F. Guinea, and A. H. Castro Neto, Rev. Mod. Phys. **84**, 1067 (2012).

[35] S. Das Sarma, S. Adam, E. H. Hwang, and E. Rossi, Rev. Mod. Phys. **83**, 407 (2011).

[36] The plasmon contribution to drag is negligible for $T < 0.15\varepsilon_F$ in both 1D [17] and 2D [15] double graphene structures.

[37] Note that in the symmetric systems of double metallic CNTs, the Fermi liquid theory of drag will diverge due to the presence in the formula (1) the product of two δ functions from Eq. (6). Meanwhile, the theory remains finite in dimensionally hybrid graphene structures.